A Sum-frequency generation from CO on the Ni/Cu(100) system

In parallel with the measurements performed on the Gd(0001) and Y(0001) systems I have developed a pilot experiment in which the CO molecules adsorbed on top a thin ferromagnetic films of Ni/Cu(100) are studied by means of sum-frequency generation technique. For this purpose I have build up a new UHV system devoted to thin films preparation and characterization as well as optical spectroscopy, and designed the optical scheme for the nonlinear optical measurements. The tool of choice in this experiment is the infrared visible sum-frequency generation, that is a widely used investigation technique for vibrational dynamics of the molecular adsorbates [97].

Unfortunately due to the unavailability of the laser system which provides laser pulses with wavelengths in the far-infrared region, the SFG measurements have been postponed until the end phase of this thesis. However, the magnetic characterization of the Ni/Cu(100) thin films with the help of MOKE as well as the study of the adsorption energetics of the CO on the epitaxial Ni films employing TDS, have been performed. Also, preliminary SFG measurements of CO/Cu(100) and CO/Ni/Cu(100) have been made, the whole work being in progress. The shown SFG spectra have been measured by my colleagues H. Öström and M. Krenz, that have joined lately this project.

The appendix is structured as follows. The UHV chamber and the laser system are briefly described followed by the Ni films preparation procedure and their magneto-optical characterization. Next the TDS measurements on the Ni thin films are showed and compared to the available data for bulk Ni crystals. In the remainder of the appendix the first SFG results are shown.

The basic idea of the experiment is to use the underlying ferromagnetic thin film in order to magnetically polarize the molecular adsorbate, here the CO molecules, and to measure the SFG signal coming from the CO stretching vibration for opposite magnetization directions. In other words, to investigate the existence of a magnetic contrast in the SFG intensity and presumably for a change of the energetic position of the SFG resonance upon magnetization reversal. As a model system for the ferromagnetic support of the adsorbate, thin films of Ni on a Cu(100) substrate have been chosen. This system provides the freedom of choosing the direction of magnetization according to the spin reorientation transition (SRT) [186], that takes place as a function of the Ni film thickness. According to literature [186, 187], below $\approx$7 ML Ni/Cu(100) the magnetization direction lies in the plane of the film whereas for higher thicknesses is oriented to an out-of-plane direction. The magnetization reorientation to an in-plane direction takes place above $\approx$35 ML [188]. Details about the origin of the SRT in Ni/Cu(100) are given latter in the Appendix.

A schematic illustration of the experiment is shown in the figure A.1. On the left side of the figure the studied system and the investigation technique are sketched. Varying the Ni
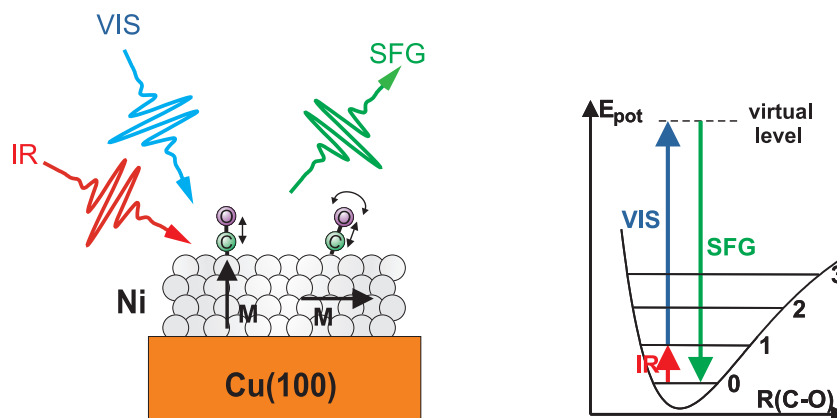
Figure A.1: Left: Schematic illustration of the SFG process and the investigated system CO adsorbed on Ni thin films on a Cu(100) substrate. As a function of Ni film thickness the magnetization reorients from in-plane to out-of-plane direction that can affect the vibrational dynamics and the adsorption geometry of the CO molecules. **Right:** The generation of the resonant SFG process in the case of CO molecule with the IR photon energy matching the energy difference between two vibrational levels of the molecule.

film thickness the orientation of magnetization M can be changed which might affect the vibrational dynamics and the geometry of the adsorbed CO molecule. The SFG process is used to detect the vibrational dynamics of the adsorbate with the infrared beam photon energy matching the intramolecular vibrational transition of the adsorbed molecule. As a result the SFG process is resonantly enhanced. This is illustrated on the right side of the figure A.1, where the vibrational potential of the CO molecule and the optical transitions of the three photons involved in the SFG process are shown.

The CO molecule chemisorbed on the Ni surface, and in general on metals, with the C atom pointing downwards. Bonding is determined by the hybridization of the 3d levels of the Ni metal with the CO 5σ and $2\pi^*$ orbitals. In the gas phase CO is diamagnetic, but upon chemisorption on the ferromagnetic Ni(100) surface, magnetic signals arising from the CO molecule could be detected by XMCD [189, 190]. The magnetic XMCD measured on 10 ML Ni/Cu(100) (out-of-plane magnetization) at the O $1s\rightarrow$ CO $2\pi^*$ transition revealed the parallel alignment of an CO $2\pi^*$ orbital moment with the Ni film magnetization [190]. For a Ni film (6 ML) with in-plane magnetization the CO $2\pi^*$ orbital moment is interpreted to be antiparallel relative to film magnetization. For the latter case, in order to maintain the hybridization with Ni atom, the CO should tilt with an angle of $\approx 30°$ with respect to surface normal [189].
The goal of this project is to detect by means of SFG the effect of the induced magnetization in CO molecule, and if successful to proceed to time-resolved measurements.

UHV chamber and the laser system

The UHV chamber is pumped by a turbomolecular pump (PFEIFFER) together with a pumping stage (PFEIFFER) consisting of a turbomolecular and a membrane pump acting
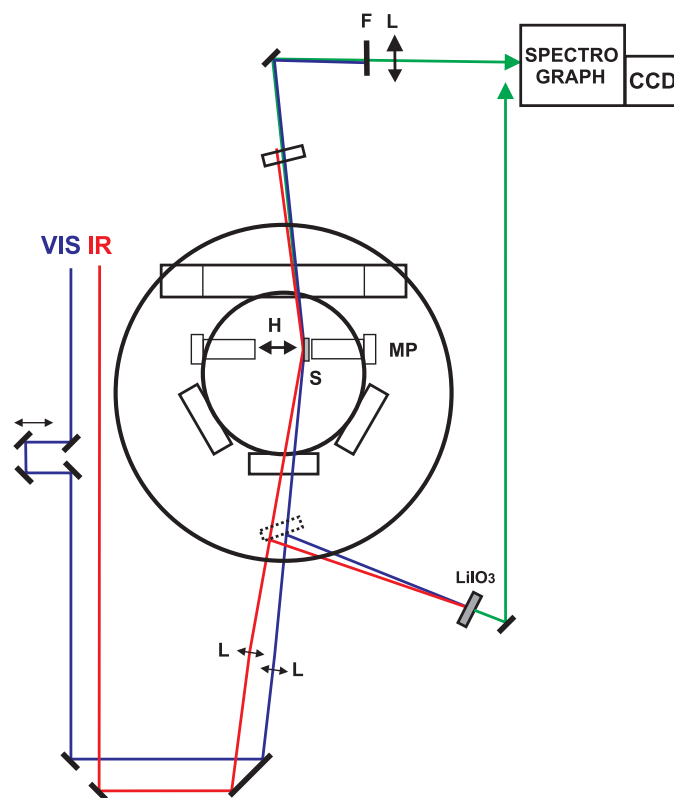
Figure A.2: Overview of the SFG optical scheme and the UHV chamber. The IR and the VIS are guided to the UHV chamber by gold-coated and dielectric mirrors, respectively, and focused to the sample (S) at $\approx 78°$ angle of incidence. The spatial and temporal overlap of the IR and VIS pulses on the sample is checked by mimicking the sample with a $LiIO_3$ nonlinear crystal that generates a SFG reference signal. The SFG signal generated on the Ni surface and by the reference crystal are directed to the detector stage formed by a monochromator and a CCD camera. A notch filter is used in order to filter-out the VIS beam. The SFG signal is measured for opposite directions of the external magnetic field H. The sample is positioned between the magnetic poles MP.

as a pre-vacuum pump. After a careful baking of the chamber the achievable base pressure is in the upper 10^{-11}mbar range.

The UHV chamber is structured on two levels: one for preparation and characterization of the thin films and a specially designed one for the optical measurements. In the preparation level an electron-beam evaporator with a quartz microbalance for thickness measurements, an electron gun together with an Ar dosing valve for sputtering, a LEED device, a quadrupole-mass spectrometer and a dosing gas system are mounted.

The optical level has a special off-axis construction that allows a sample positioning close to the entrance window used for guiding the laser beams to the sample. Employing short focal distance optics a better focusing can be achieved and thus a considerable increase of the incident laser fluence. Such a chamber design is useful for the nonlinear optical measurements where the laser focus is a parameter that can increase the efficiency
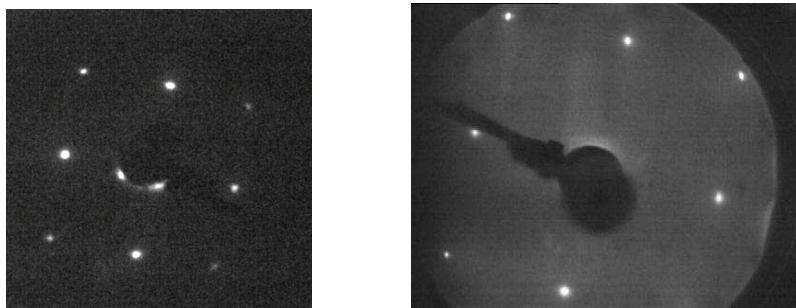
Figure A.3: The LEED patterns obtained from a clean Cu(100) substrate (left) and a 7 ML Ni film (right) at 153 eV and 140 eV beam energy, respectively. Both spectra are recorded at room temperature.

of the nonlinear process (see eq....). In the optical level a home-made electromagnet is installed. This is specially designed with the poles situated in vacuum, mounted uninterrupted through the chamber flanges and closing the loop outside the chamber where the coils are installed. By this construction, high currents can be used for producing the magnetic field with no risk of contaminating the vacuum by outgassing. The maximum obtainable magnetic field is $\approx$250 gauss measured in the middle of the electromagnet gap, which has a 36 mm length. The strength of the external magnetic field is sufficient in order to magnetize the Ni films in saturation along the magnetization easy axis. This electromagnet design allows magneto-optical measurements in the polar and longitudinal configurations (see figure 3.5).

For the magnetic characterization of the grown Ni films I have constructed a MOKE polarimeter designed in the balanced detection configuration [113]. This construction is particularly useful for detecting ultrathin ferromagnetic films since the possible laser fluctuations are single out. The sensitivity of the MOKE detector is in the atomic monolayer range.

At the preparation level a home-made evaporator is installed, with the evaporation material under the form of Ni wires (99.99% purity) mounted in a W crucible. The crucible has been extensively outgassed before using. The evaporation is realized by electron-beam heating with the crucible and the filament mounted in a water-cooled Cu shroud.

The QMS is used for TDS measurements and residual-gas analysis. The CO is dosed on the sample using a gas dosing system consisting of leak valve and a metallic tube extended into the chamber. The sample can be positioned very close to the dosing tube and thus avoiding to expose other parts of the sample holder to the dosed adsorbate. A rough estimation of the dosed adsorbate quantity is made by reading the ion gauge pressure and the time of dosing.

The laser system used for the SFG measurements consists of an Ti:Sa oscillator (Coherent Vitesse) that seeds an regenerative amplifier (Quantronix Titan II). The amplified laser pulses are used in the generation of the far infrared pulses by employing a commercial system (TOPAS) in which several nonlinear processes (optical parametric generation and amplification, difference frequency generation) are involved. The output IR pulses are
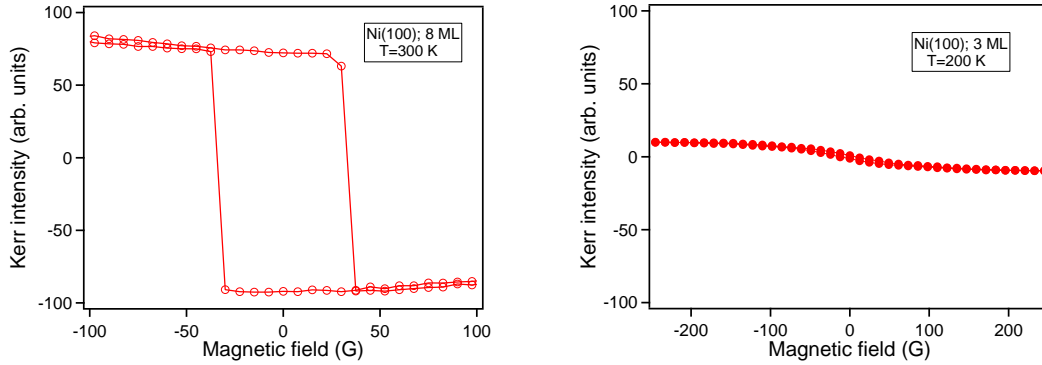
Figure A.4: The MOKE spectra measured on 8 ML and 3 ML Ni film thickness at a sample temperature of 300 K and 200 K, respectively, in the polar configuration with a s-polarized laser beam.

tunable between 2.4 and 10 μm, $\approx$150 fs in duration, with a pulse energy of 15 μJ. The VIS laser beam used for SFG up-conversion process is centered at 800 nm wavelength, a pulse duration of 5 ps and energy per pulse around 15 μJ. For more details about the laser system the reader is referred to the Daniel Denzler's thesis [191].

Ni thin films preparation and characterization

The Cu(100) substrate is cleaned by repeated cycles of Ar^+ sputtering at 1 KeV energy and subsequent annealing to 850 K for 5 minutes. The cleanliness and the crystalline quality of the substrate has been checked by LEED. The LEED picture obtained for a clean Cu(100) substrate at a beam energy of 153 eV is displayed in the left part of the figure A.3.

Epitaxial Ni thin films with thicknesses ranging from 3 ML (1 ML=1.7Å) to 30 ML have been prepared using a similar method as reported by Shen *et al.* [192]. This consists in depositing the Ni on the Cu(100) substrate held at room temperature at a $\approx$1 Åmin deposition rate followed by annealing to 420 K for 5 minutes. By this method smooth Ni films have been obtained as can be judged from the LEED picture displayed on the right part of the figure A.3. Higher annealing temperatures (above 450 K) are not recommended since for this system significant atomic inter-diffusion from the substrate to the film surface can occur.

MOKE measurements

The film growth of Ni on the Cu(100) substrate is pseudomorph with a face-centered tetragonal (fct) Ni lattice, up to $\approx$11 ML [187] film thickness. This is due to the film/substrate lattice mismatch that amounts to 2.5%, the Ni layers becoming strained in order to match the Cu(100) lattice. For higher thicknesses the strain induced by the lattice mismatch is released by defects (misfit dislocations) and the lattice symmetry is relaxed to the normal face-centered cube (fcc) type. This tetragonal distortion of the lattice is the origin of the spin-reorientation transition that take place on the Ni/Cu(100) system in the low thickness

range [186]. More detailed, in ferromagnetic thin films the orientation of magnetization is determined by the interplay among different magnetic anisotropy terms, whose magnitude can change with temperature, film thickness etc. In general, an out-of-plane magnetization orientation is favored when the following condition is fulfilled [188]:

$$K_V + \frac{K_S + K_i}{d} > 2\pi M^2 \tag{A.1}$$

where d is the film thickness, M the saturation magnetization and K_V, K_S and K_i represent the second-order magnetization anisotropy energy terms of bulk (volume), surface and interface regions, respectively. The right-hand term denotes the shape anisotropy energy of magnetic dipolar origin. The tetragonal distortion produces a uniaxial anisotropy that increases the value of the volume K_V anisotropy term [186] and thus overcoming the the negative value of K_S and shape anisotropy, the latter one being favorable to an in-plane magnetization orientation. As a result the magnetization orients from in-plane to out-of-plane direction.

In the figure A.4 the MOKE measurements for two different Ni film thicknesses are displayed. The MOKE hysteresis are measured in polar configuration (magnetization in the plane of incidence and normal to the surface) with a s-polarized laser beam. In the polar configuration one thus detects the out-of-plane component of the magnetization M_z. We observe a square shape of the hysteresis for the 8 ML NI film whereas for the 3 ML we notice a hysteresis with no coercivity. The former one indicates a measurement along easy axis whereas the latter one shows a shape that is typical for measurements performed along hard-axis of magnetization. From here one can conclude that for the 8 ML Ni film the magnetization orientation is out-of-plane while for the 3 ML thickness is having an in-plane direction. Higher Ni film thicknesses (up to 30 ML) have been investigated (not shown) showing larger coercivity but no significant change in the shape of the hysteresis loop *i.e.* square-like, indicating an out-of-plane magnetization direction.

TDS CO on Ni(100) thin films

The next step was to investigate the adsorption energetics of the CO molecules on the Ni thin films and to study which is the optimal film thickness in terms of adsorption sites occupation. No TDS measurement are reported in literature for CO adsorbed on epitaxial Ni films just on Ni bulk single crystals [193, 194]. For bulk crystals the CO TDS measurements reveal [193] three desorption sites at 450 K , 350 K and 280 K labelled as β_2, β_1 and α, respectively. In the same study the adsorption sites of the CO molecules have been identified employing Fourier transform infrared adsorption spectroscopy (FTIRA): at low temperatures (around 200 K) the bridge sites adsorption is favored while for temperatures above 300 K the terminal (on-top) sites are preferred. The high temperature desorption peak is considered [194] to arise from the on-top adsorbed CO while the other peaks are attributed to bridge and hollow sites. For our experiment is important to prepare samples with an ordered adsorbate structure in order to have a narrow signature in the vibrational spectra. For the case of CO on Ni(100) a c(2x2) structure is obtained upon dosing the CO saturation coverage followed by a short annealing to 330 K. The same procedure is used for the clean Cu(100) substrate in obtaining the c(2x2) structure, but for a short annealing to 140 K.
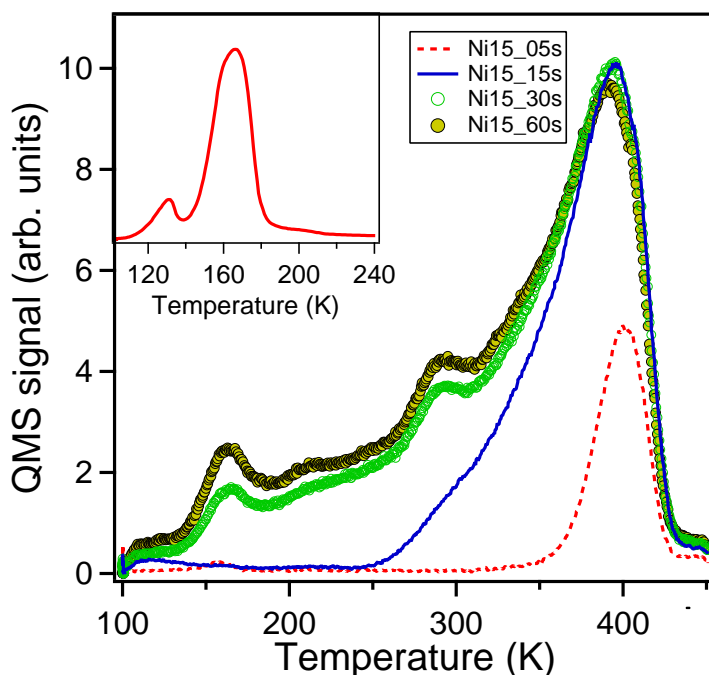
Figure A.5: TDS measurements of the CO adsorbed on a 15 ML Ni film at 100 K, performed at various CO coverages and a heating rate of 1.67 K/sec. The coverages are indicated by the exposure time in seconds at a background pressure of $2x10^{-10}$mbar. In the inset the TDS spectrum measured on the Cu(100) substrate for the saturation coverage of CO.

In the figure A.5 the TDS spectra measured on a 15 ML Ni/Cu(100) film are displayed. The CO is dosed at 100 K by monitoring the background pressure and the time of dosing. We observe three peaks that can be attributed to the desorbed species from Ni: the 400 K, 290 K and the weak one at 210 K. The lower temperature desorption peaks are from the Cu sample as can be deduced by comparing them with the TDS data measured on the clean Cu(100) substrate (see the inset of the figure A.5). Comparing the measured TDS spectra on the Ni thin films to the corresponding data on the bulk Ni crystal [193, 194], we notice a shift to lower temperatures of the desorption peaks. On a speculative level one can ascribe this behavior to the presence of higher density of defects induced by strain release, that could reduce the adsorption energy of the CO on the Ni film. We have investigated also Ni films of higher thicknesses in order to check the influence of the increased roughness on the CO adsorption. The measured TDS spectra for various Ni film thicknesses are displayed in the figure A.6. The plotted spectra correspond to the CO saturation coverage of the on-top site *i.e.* the 400 K desorption peak in the figure A.5. By increasing the thickness from 15 ML to 30 ML we observe a gradual intensity increase of the TDS β_1 peak (presumably bridge sites) at the extent of β_2 peak (presumably on top sites), and for the 30 ML Ni film becomes dominant adsorption site. This is an interesting observation that requires further investigations.

Based on these measurements and literature data, that report the strain release starting
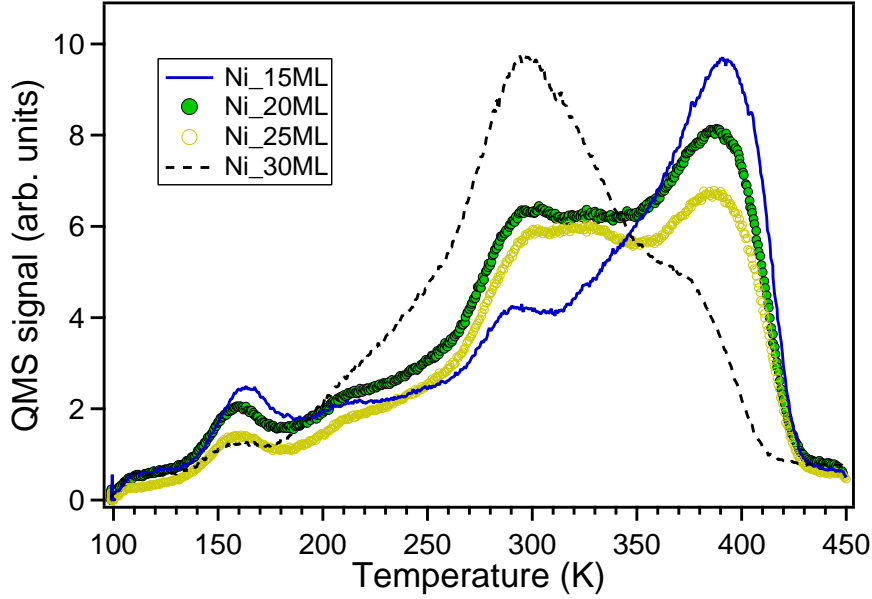
Figure A.6: TDS spectra measured for the saturation CO dosage (the 60 sec exposure time spectrum in the figure A.5) for various Ni film thicknesses.

with the 11 ML Ni film thickness, we decided that the thickness around 10-11 ML to be the optimal one for the SFG measurements.

SFG theory and experiment

As detailed in chapter 3, sum-frequency generation is a second-order nonlinear optical process, in which, unlike SHG, the involved photons have different frequencies. Thus one can write the nonlinear optical polarization responsible for the SFG process as:

$$P^{(2)}(\omega_{SFG}) = \chi^{(2)}_{SFG}E(\omega_1)E(\omega_2) \tag{A.2}$$

with the $\omega_{SFG} = \omega_1 + \omega_2$ representing the outgoing sum-frequency photon as a sum of the two input photons frequencies. Similar to the SHG the SFG process is forbidden (within electric-dipole approximation) in the centrosymmetric media and thus allowed only in spatial regions with broken inversion symmetry *e.g.* surfaces, interfaces etc. For the investigation of the molecular vibrations the broadband infrared (IR) visible (VIS) sum-frequency generation technique is widely employed [195, 196], with a tunable IR beam through vibrational resonances of the adsorbed species and with the VIS beam used for up-converting the resulting SFG signal to visible range. Thus one can write the second-order susceptibility as the sum of a resonant and non-resonant term [196]:

$$\chi^{(2)}_{SFG} = \chi^{(2)}_{R} + \chi^{(2)}_{NR} = \sum_q \frac{A_q}{\omega_{IR} - \omega_q + i\Gamma_q} + A_0 e^{i\phi} \tag{A.3}$$
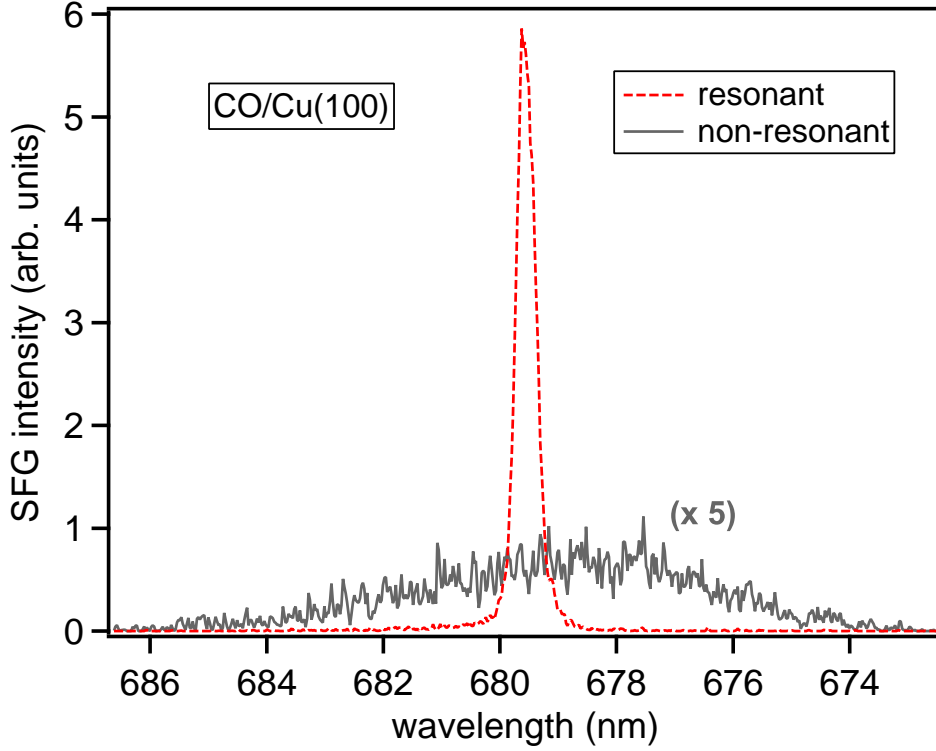
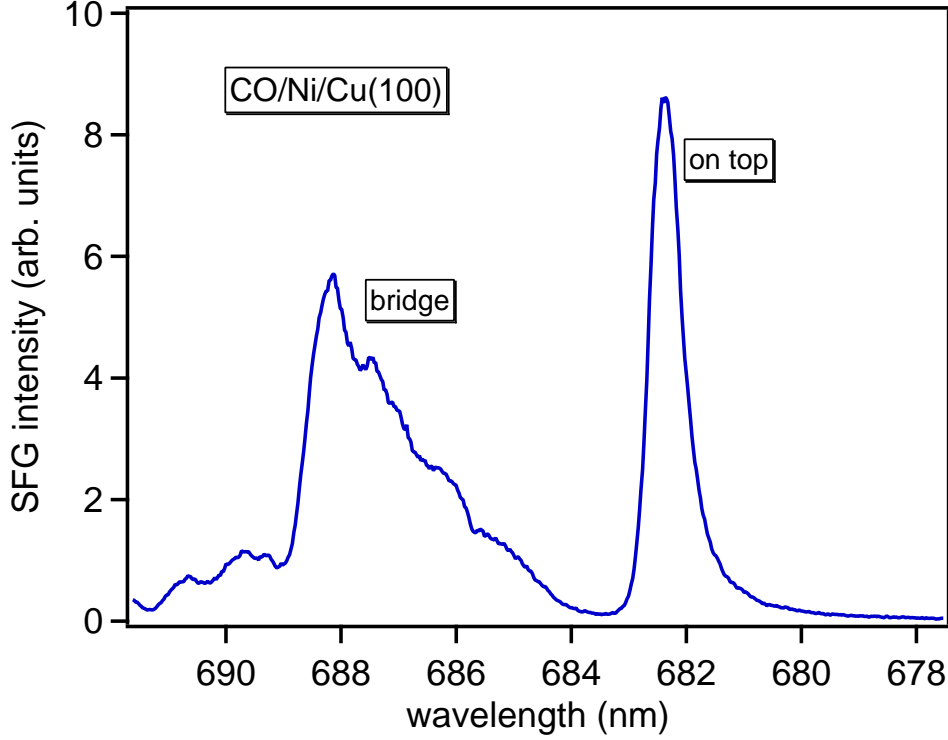**Figure A.7:** The SFG spectra measured at T=100 K arising from the CO resonance adsorbed on Cu(100) and from the non-resonant background generated by the clean Cu(100) substrate.

where the A_q, ω_q, ω_{IR}, Γ_q denote the amplitude and the resonant frequency of the q-th vibrational mode, the infrared laser frequency, the damping constant of the vibrational mode ($2\Gamma_q$ is the linewidth), respectively. A_0 is the amplitude of the non-resonant susceptibility and ϕ is its phase with respect to the resonant susceptibility. The amplitude of the vibrational mode is defined as: $A_q = (2\omega_q)^{-1}\frac{\partial\mu}{\partial q}\frac{\partial\alpha}{\partial q}$ where μ and α represent the dipole moment and the linear polarizability. This relation shows that a vibrational mode can be measured by SFG when is simultaneously infrared and Raman active.

As for the SHG case the susceptibility tensor has 27 components that can by reduced by applying the symmetry operations of the particular system. For the case of fcc Ni(100) the symmetry (C_{4v}) is identical to an isotropic surface and the resulting non-vanishing tensor components are:

$$\chi_{xzx} = \chi_{yzy}; \quad \chi_{xxz} = \chi_{yyz}; \quad \chi_{zxx} = \chi_{zyy}; \quad \chi_{zzz}$$

The presence of the magnetization lowers the symmetry of the system and the number of non-vanishing tensor components is increased, with the tensor components behaving even and odd with respect to magnetization reversal (see chapter 3). For the case of polar geometry, with $M \parallel z$ and the plane of incidence in the (xz) plane, the SFG susceptibility

Figure A.8: The SFG spectra arising from the CO resonance adsorbed on 11 ML Ni/Cu(100) measured at T=100 K. Note the distinct peaks with central frequencies of 2000 cm^{-1} and 1894 cm^{-1} corresponding to the on top and bridge adsorbed species, respectively.

tensor takes the following form:

$$
\begin{pmatrix}
0 & 0 & \chi_{xxz}^{even} & 0 & 0 & \chi_{xyz}^{odd} & \chi_{xzx}^{even} & \chi_{xzy}^{odd} & 0 \\
0 & 0 & \chi_{yxz}^{odd} & 0 & 0 & \chi_{yyz}^{even} & \chi_{yzx}^{odd} & \chi_{yzy}^{even} & 0 \\
\chi_{zxx}^{even} & \chi_{zxy}^{odd} & 0 & \chi_{zyx}^{odd} & \chi_{zyy}^{even} & 0 & 0 & 0 & \chi_{zzz}^{even}
\end{pmatrix}
\tag{A.4}
$$

In order to have a magnetic induced SFG signal one has to look for the proper magneto-optical geometry and polarization combinations. Sine we are interested on the M_z component of the magnetization, we stay in the polar geometry and choose the polarization configuration with the highest number of even and odd tensor components. This experimental geometry is (P45°P) or (total45°P), where the letters represent the polarization of the SFG, VIS and the IR beam, respectively. The "total" denotes the SFG signal detection without analyzing its output polarization.

Before measuring the SFG signal from the Ni film a test measurement has been performed on the clean Cu(100) substrate. The wavelength of the VIS and IR beams were 790 nm and 5 μm, respectively. The result is plotted in the figure A.7, showing the resonant and the non-resonant SFG signals arising from the on top CO stretching vibration and the free electrons response, respectively. As expected, the CO resonance is energetically positioned at 2035 cm^{-1} and has a FWHM of 11 cm^{-1}.

Only recently, the very first SFG measurements of CO adsorbed on the Ni thin films have started, showing a magnetic contrast of $\approx 1\%$ in the MSFG signal arising from the CO stretching vibration. Such a measurement is displayed in figure A.8, where we observe the vibrational signature of the on top and bridge species at ≈ 2000 cm^{-1} and ≈ 1894 cm^{-1}, respectively. These values are slightly lower than the reported (coverage dependent) data in literature for bulk Ni [193]: between 2010-2050 cm^{-1} for the on top and 1910-1970 cm^{-1} for the bridge sites. These measurements are in progress and upon improving the experimental parameters better results are expected. These results show the potential of this technique that can be applied to other magnetic systems. A very interesting fact will be to investigate in a time-resolved manner the spin-polarization of the CO molecules on Ni films employing the MSFG.

B Fitting procedure

In the following, the procedure used for data analysis of the time-resolved linear reflectivity and second-harmonic generation transients is presented in detail. The main purpose of this procedure is to extract the oscillatory component of the transient signal in a correct manner out of the raw data. This could not be achieved by simply fitting the incoherent background with a pre-defined function like exponential or low order polynomial since the former one could not well reproduced the non-oscillatory background and the latter one introduces fitting artifacts at the limits of the fitted data range. Also one needs a criterion to judge if the separation of the oscillatory and non-oscillatory components is correct and eventually the data analysis is reliable. This procedure has been developed by Alexey Melnikov for a quantitative evaluation of the oscillatory component encountered in the time-resolved LR and SHG signals.

The expression of the oscillatory component of the signal has been defined in eq. 5.8, which describes an exponentially damped cosine function. For a better understanding of the data analysis procedure this expression is reproduce here once again:

$$f(t) = Ae^{-t/\tau} \cdot \cos[2\pi(\Omega \cdot t + c \cdot t^2 + \varphi)] \tag{B.1}$$

with A, τ, Ω and φ being the amplitude, decay time, frequency and the phase, respectively.

The first step in the data analysis is smoothing the original data E_d. This step is necessary especially for the data sets with a low signal to noise ratio obtained *e.g.* at high temperatures (see fig B.2). Smoothing is carried out by fitting the original data with a polynomial function in a certain time window *i.e.* each data point is replaced by the value of the polynomial fitted to the data. The order of the polynomial function i and the number of points j within the time window (pump-probe delay steps) are optimized by an *autocorrelation* criterion, that optimizes the *non-randomness* in the resulting smoothed data set. That means the noise is filtered while keeping the correct representation of the oscillatory part of the signal. The time window is shifted along the time axis of the original data set and a subsequent averaging over the window position is preformed, that results in the smoothed curve E_s. The noise level E_n is obtained straightforward making the difference between E_d and E_s.

In the next step the incoherent part of the transient data is evaluated. For this, the expression B.1 is subtracted from the smoothed data by optimizing the parameters A, τ, Ω and φ in order to get a minimum of the mean square of the second derivative of the resulting expression: $E_{sub} = E_s - Ae^{-t/\tau} \cdot \cos[2\pi(\Omega \cdot t + c \cdot t^2 + \varphi)]$ with $\left\langle \left(\frac{\partial^2 E_{sub}}{\partial t^2}\right)^2 \right\rangle \longrightarrow$ min.

Here we have to mention that we made an *a-priori* assumption regarding the oscillatory profile of the expression B.1, that reproduces the original oscillatory signal. The incoherent background E_b is obtained using the same autocorrelation criterion applied now to E_{sub}
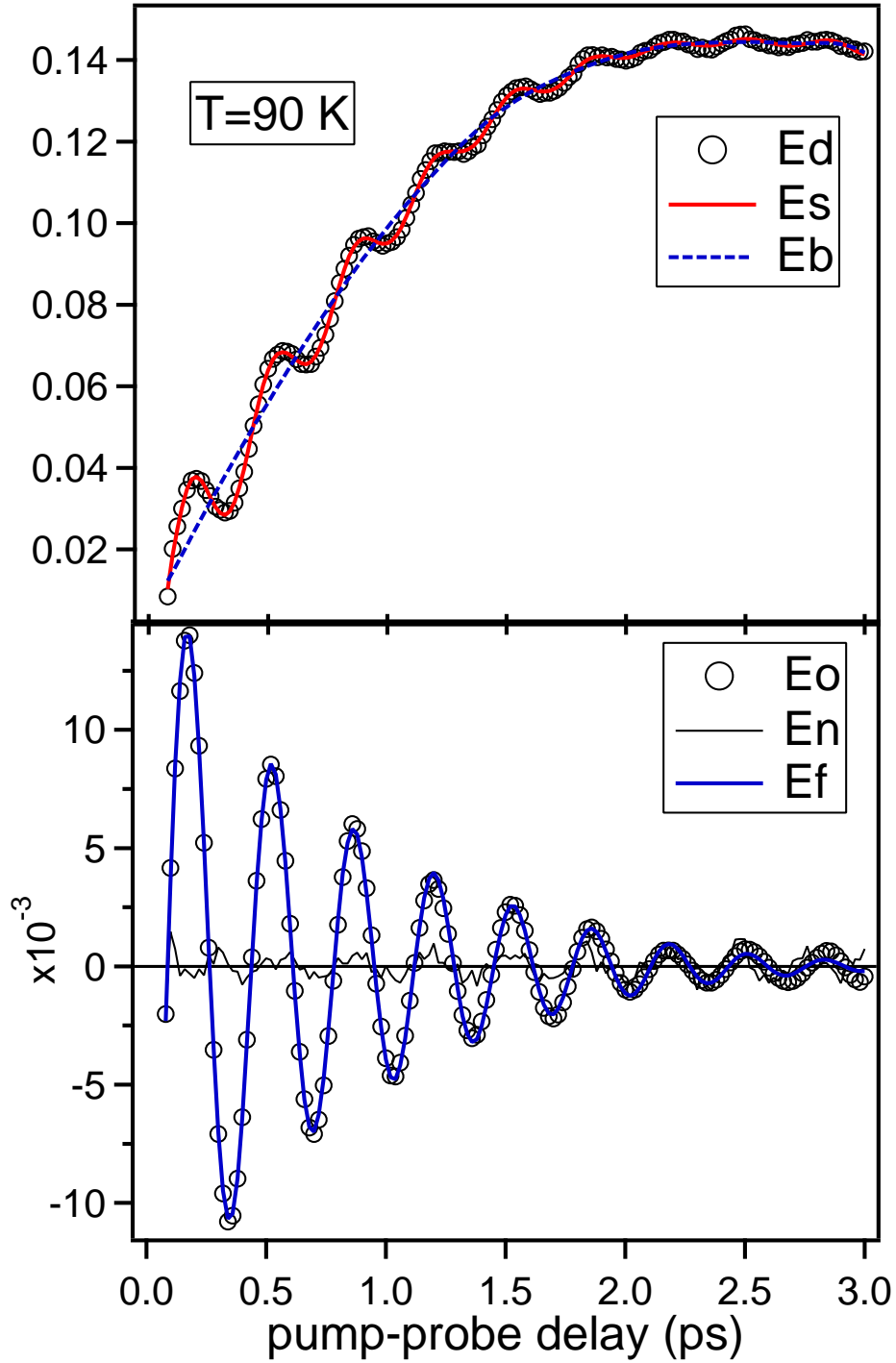
Figure B.1: Exemplary data set showing the pump-induced variations in the even SH field measured at 90 K as well as the relevant quantities involved in the data analysis procedure. In the upper panel the E_d, E_s, E_b denote the original data, the smoothed curve and the non-oscillatory background, respectively. In the lower panel E_o, E_n, E_f describe the resulting oscillatory data, the noise and the fit according to B.1, respectively.
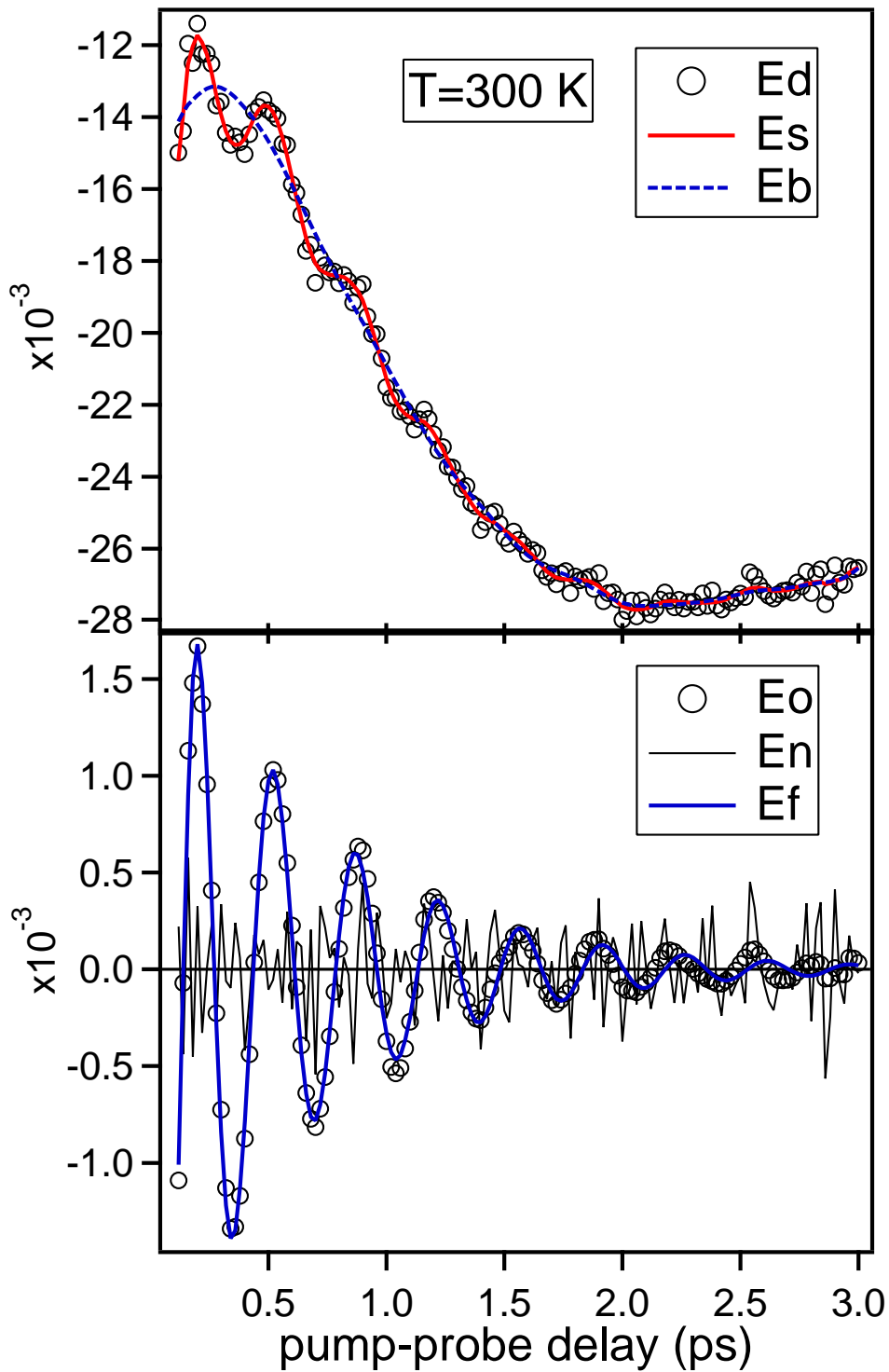
Figure B.2: The same as in figure B.1 but for a measurement performed at 300 K. Note the different time-evolution of the incoherent background and the higher level of noise.

but inverted using a low polynomial degree and a larger time-window *i.e.* having the optimal window size condition fulfilled:

$$\frac{\langle (E_b - E_{sub})^2 \rangle}{\langle (P - E_{sub})^2 \rangle} + \frac{\langle (\ddot{E}_b - \ddot{P})^2 \rangle}{\langle (\ddot{E}_{sub} - \ddot{P})^2 \rangle} \sqrt{\frac{\langle \ddot{E}_{sub}^2 \rangle}{\langle \ddot{P}^2 \rangle}} \longrightarrow min \tag{B.2}$$

where $P(t)$ is the polynomial fit to $E_{sub}(t)$.

The final stage is to obtain the oscillatory component E_o of the data. E_o is retrieved by subtracting the incoherent background E_b from the smoothed original data E_s. Now one can fit the oscillatory data E_o with the expression B.1 in order to get the values of the parameters A, τ, Ω and φ.

In order to show how the fitting procedure works two exemplary data sets have been chosen, measured at low and elevated temperatures *i.e.* a lower and higher level of noise, respectively. The displayed measurements are performed under identical conditions: incident laser beams parameters, film thickness etc.